

Dynamic saturation in semiconductor optical amplifiers: accurate model, role of carrier density, and slow light

Perrine Berger^{1,2}, Mehdi Alouini^{1,3}, Jérôme Bourderionnet¹,
Fabien Bretenaker², and Daniel Dolfi¹

¹Thales Research & Technology, 1 av. Augustin Fresnel, 91767 Palaiseau Cedex, France

²Laboratoire Aimé Cotton, CNRS-Université Paris Sud 11, Campus d'Orsay, 91405 Orsay Cedex, France

³Institut de Physique de Rennes, UMR CNRS 6251, Campus de Beaulieu, 35042 Rennes Cedex, France

Perrine.Berger@thalesgroup.com

Abstract: We developed an improved model in order to predict the RF behavior and the slow light properties of the SOA valid for any experimental conditions. It takes into account the dynamic saturation of the SOA, which can be fully characterized by a simple measurement, and only relies on material fitting parameters, independent of the optical intensity and the injected current. The present model is validated by showing a good agreement with experiments for small and large modulation indices.

© 2018 Optical Society of America

OCIS codes: (250.5980) Semiconductor optical amplifiers; (070.6020) Continuous optical signal processing.

References and links

1. J. Yao, "Microwave Photonics," *J. Lightwave Technol.* **27**, 314-335 (2009).
2. D. Dolfi, P. Joffre, J. Antoine, J-P. Huignard, D. Philippet, and P. Granger, "Experimental demonstration of a phased-array antenna optically controlled with phase and time delays," *Appl. Opt.* **35**, 5293-5300 (1996).
3. J. Capmany, B. Ortega, and D. Pastor, "A Tutorial on Microwave Photonic Filters," *J. Lightwave Technol.* **24**, 201-229 (2006).
4. C. J. Chang-Hasnain and S. L. Chuang, "Slow and Fast Light in Semiconductor Quantum-Well and Quantum-Dot Devices," *J. Lightwave Technol.* **24**, 4642-4654 (2006).
5. H. Su, and S. L. Chuang, "Room temperature slow and fast light in quantum-dot semiconductor optical amplifiers," *App. Phys. Lett.* **88**, 061102 (2006).
6. A. V. Uskov, F. G. Sedgwick, and C. J. Chang-Hasnain, "Delay Limit of Slow Light in Semiconductor Optical Amplifiers," *IEEE Photon. Technol. Lett.* **18**, 731-733 (2006).
7. B. Pesala, F. Sedgwick, A. Uskov, and C. Chang-Hasnain, "Ultrahigh-bandwidth electrically tunable fast and slow light in semiconductor optical amplifiers," *J. Opt. Soc. Am. B* **25**, C46-C54 (2008).
8. L. Thévenaz, "Slow and fast light in optical fibres," *Nature Photonics* **2**, 474-481 (2008).
9. P.-C. Ku, F. Sedgwick, C.J. Chang-Hasnain, P. Palinginis, T. Li, H. Wang, S.-W. Chang, and S-L. Chuang, "Slow light in semiconductor quantum wells," *Opt. Lett.* **29**, 2291-2293 (2004).
10. R. Boula-Picard, M. Alouini, J. Lopez, N. Vodjdani, and J.-C. Simon, "Impact of the Gain Saturation Dynamics in Semiconductor Optical Amplifiers on the Characteristics of an Analog Optical Link," *J. Lightwave Technol.* **23**, 2420-2426 (2005).
11. J. Mørk, R. Kjr, M. van der Poel, and K. Yvind, "Slow light in a semiconductor waveguide at gigahertz frequencies," *Opt. Express* **13**, 8136-8145 (2005).
12. S. S. Maicas, F. Öhman, J. Capmany, and J. Mørk, "Controlling Microwave Signals by Means of Slow and Fast Light Effects in SOA-EA Structures," *IEEE Photon. Technol. Lett.* **19**, 1589-1591 (2007).

13. Y. Chen, and J. Mørk, "Broadband Microwave Phase Shifter based on High Speed Cross Gain Modulation in Quantum Dot Semiconductor Optical Amplifiers," in *International Topical Meeting on Slow and Fast Light*, 2009 OSA Technical Digest (Optical Society of America, 2009).
14. G. P. Agrawal, "Population pulsations and nondegenerate four-wave mixing in semiconductor lasers and amplifiers," *J. Opt. Soc. Am. B* **5**, 147-159 (1988).
15. E. Zhou, X. Zhang, and D. Huang, "Evaluating characteristics of semiconductor optical amplifiers using optical pumping near the transparency," *J. Opt. Soc. Am. B* **24**, 2647-2657 (2007).
16. A. Capua, V. Mikhelashvili, G. Eisenstein, J. P. Reithmaier, A. Somers, A. Forchel, M. Calligaro, O. Parillaud, and M. Krakowski, "Direct observation of the coherent spectral hole in the noise spectrum of a saturated InAs/InP quantum dash amplifier operating near 1550 nm," *Opt. Express* **16**, 2141-2146 (2008).
17. J. Kim, M. Laemmlin, C. Meuer, D. Bimberg, and G. Eisenstein, "Static Gain Saturation Model of Quantum-Dot Semiconductor Optical Amplifiers," *IEEE J. Quantum Electron.* **44**, 658-666 (2008).
18. S.-W. Chang, P. K. Kondratko, H. Su, and S. L. Chuang, "Slow Light Based on Coherent Population Oscillation in Quantum Dots at Room Temperature," *IEEE J. Quantum Electron.* **43**, 196-205 (2007).
19. M. J. Connelly, "Wideband Semiconductor Optical Amplifier Steady-State Numerical Model," *IEEE J. Quantum Electron.* **37**, 439-447 (2001).
20. Y. Chen, W. Xue, F. Ohman, and J. Mork, "Theory of optical-filtering enhanced slow and fast light effects in semiconductor optical waveguides," *Lightwave Technology, Journal of* **23**, 3734-3743 (2008).
21. T. Mukai and T. Saitoh, "Detuning characteristics and conversion efficiency of nearly degenerate four-wave mixing in a 1.5- μm traveling-wave semiconductor laser amplifier Quantum Electronics," *Quantum Electronics, IEEE Journal of* **16**, 865-875 (1990).
22. A. Haug, "Evidence of the importance of auger recombination for InGaAsP lasers," *IEE Electron. Lett.* **20**, 85-86 (1984).
23. E. Rosencher and B. Vinter, *Optoelectronics* (Cambridge, 2002).
24. M. Shtaif, B. Tromborg, and G. Eisenstein, "Noise spectra of semiconductor optical amplifiers: relation between semiclassical and quantum descriptions," *Quantum Electronics, IEEE Journal of* **34**, 869-878 (1998).
25. A. Ouacha, Q. Chen, M. Willander, R. A. Logan, and T. Tanbun-Ek, "Recombination process and its effect on the dc performance of inp/ingaas single-heterojunction bipolar transistors," *Journal of Applied Physics* **73**, 444-4447 (1993).
26. L. Y. Leu, J. T. Gardner, and S. R. Forrest, "A high-gain, high-bandwidth $\text{In}_{0.53}\text{Ga}_{0.47}\text{As}/\text{InP}$ heterojunction phototransistor for optical communications," *Journal of Applied Physics*, **69**, 1052-1062 (1991).
27. E. A. J. M. Bente, Y. Barbarin, M. J. R. Heck, and M. K. Smit, "Modeling of integrated extended cavity inp/ingaasp semiconductor modelocked ring lasers," *Optical and Quantum Electronics*, **40**, 131-148 (2008).
28. M. Petrauskas, S. Juodkakis, V. Netikis, M. Willander, A. Ouacha, and B. Hammarlund, "Picosecond carrier dynamics in highly excited ingaas/inp/ingaasp/inp structures," *Semiconductor science and technology*, **7**, 1355-1358 (1992).
29. E. Shumakher, S. Dill, and G. Eisenstein, "Optoelectronic Oscillator Tunable by an SOA Based Slow Light Element," *Lightwave Technology, Journal of* **27**, 4063-4068 (2009).
30. S. O Duill, R. F. O'Dowd, and G. Eisenstein, "On the role of high-order coherent population oscillations in slow and fast light propagation using semiconductor optical amplifiers," *Selected Topics in Quantum Electronics, IEEE Journal of* **15**, 578-584 (2009).
31. P. Berger, J. Bourderionnet, M. Alouini, F. Bretenaker and D. Dolfi, "Theoretical Study of the Spurious-Free Dynamic Range of a Tunable Delay Line based on Slow Light in SOA," *Optics Express* **27**, 20584-20597 (2009).

1. Introduction

The generation of continuously tunable optical delays is a key element in microwave photonics. Among the targeted applications, one can quote the filtering of microwave signals, the synchronization of optoelectronics oscillators, and the control of optically fed phased array antennas [1, 2, 3]. With these applications in view, large efforts are currently done in order to develop delay lines based on slow and fast light effects [4, 5, 6, 7, 8]. To date, one of the most mature approaches for integration in real field systems is that based on Coherent Population Oscillations (CPO) in semiconductor structures [9, 10, 11]. This approach offers compactness, continuous tunability of the delay through injected current control, and possible high-level parallelism [12, 13]. Obviously, the implementation of CPO effects in microwave photonics delay lines relies on accurate theoretical description of the underlying mechanisms in order to develop reliable predictive models. Numerous theoretical models have been developed in the past few years to describe CPO effects in Semiconductor Optical Amplifiers (SOAs) [14, 15, 16, 17].

They are usually based on a semi-classical description of the interaction between the carriers and the input optical fields. These models offer a comprehensive understanding of the gain saturation dynamics and associated group index changes. However, on the one hand, a complete model would require a detailed knowledge of the geometrical and material parameters of the semiconductor structure [18, 19]. Unfortunately, most of them are unknown especially when the SOA under consideration is a commercially available device. On the other hand, others, simpler, assumed that both the saturation power and the carrier recombination lifetime are constant [5, 14, 20, 21]. This assumption applies when the SOA is operated at a fixed injection current [22, 23]. However, the injection current and the input optical power have to be tuned over a wide range in order to control the speed of light into the SOA: consequently this assumption restricts the predictive capability of a model describing microwave-photonics delay lines using slow light in SOA.

In this paper we derive an improved model that enables to predict the RF gain compression, the RF phase delay, and the optical group delay and which is valid for all experimental conditions for a given component. Furthermore, we show that the detailed knowledge of the inner geometrical and material characteristics of the SOA is not required provided that some preliminary and easy characterization measurements are conducted. This model is then experimentally validated.

2. Model

We consider an optical carrier modulated by an RF signal and injected in a traveling wave SOA. The total field is then composed of the optical carrier of complex amplitude E_0 and two sidebands of complex amplitudes E_1 and E_2 . The total optical field E is normalized to include the factor $\sqrt{\epsilon_0 n_0 c_0}$, i.e., the optical intensity is given by $I_{opt}(z, t) = \frac{1}{2} |E_{total}|^2 = U + M e^{-i\Omega t} + c.c.$, under small RF signal approximation. U is the DC component of the intensity, $M = \frac{1}{2} (E_0 E_2^* + E_1 E_0^*)$ is the beat-note term at the RF frequency Ω .

The local equations for the propagation of the optical field E_{total} and the evolution of carrier density N inside the SOA are [14]:

$$\frac{dN(z, t)}{dt} = \frac{I}{qV} - \frac{N(z, t)}{\tau_s} - \frac{g(z, t) |E_{total}(z, t)|^2}{\hbar\omega}, \quad (1)$$

$$\frac{d|E_{total}(z, t)|^2}{dz} = |E_{total}(z, t)|^2 [-\gamma + \Gamma g(z, t)], \quad (2)$$

where γ holds for the internal losses of the SOA, $\Gamma g(z, t)$ is the material modal gain, τ_s is the carrier lifetime, I is the injected current, V is the volume of the active region, and ω is the pulsation of the optical carrier E_0 . We introduce $N(z, t) = \bar{N}(z) + \Delta N(z) e^{-i\Omega t} + c.c.$ and $g(z, t) = g(N(z, t)) = \bar{g}(\bar{N}(z)) + a(\bar{N}(z)) \Delta N(z) e^{-i\Omega t} + c.c.$ where a is the differential gain $a(\bar{N}) = \frac{\partial g}{\partial N}|_{\bar{N}}$. The wavelength of the optical carrier is fixed. Consequently, the equations Eq. 1 and Eq. 2 lead to:

$$\frac{dU}{dz} = U [-\gamma + \Gamma g(\bar{N})], \quad (3)$$

$$\frac{dM}{dz} = M \left\{ -\gamma + \Gamma g(\bar{N}) \left(1 - \frac{U/U_s(\bar{N})}{1 + U/U_s(\bar{N}) - i\Omega\tau_s(\bar{N})} \right) \right\}, \quad (4)$$

where $U_s(\bar{N})$ is the saturation intensity defined as: $U_s(\bar{N}) = \frac{\hbar\omega}{a(\bar{N})\tau_s(\bar{N})}$.

In most of the simple models, the common approach to solve equations (3) and (4) is to consider a and τ_s constant with respect to the carrier density and thus over the whole length

of the device [5, 14, 20, 21]. This approximation does however not give account of strong saturation conditions, with high gain and carrier density variations, which typically occur in quantum wells structures with strong carrier confinement. In this paper, we propose to consider the carrier density variation along the propagation axis and its influence on a and τ_s . Our central hypothesis is that a and τ_s can be determined as functions of the DC component of the optical intensity U solely, allowing these dependencies to be determined from gain measurements.

Let us first suppose that we fulfill the small signal condition. In this case, the stimulated emission is negligible compared to the spontaneous emission, leading to the unsaturated steady state solution of the rate equation (Eq. 1):

$$\frac{I}{q L S_{act}} = \frac{\bar{N}}{\tau_s}, \quad (5)$$

where L is the length of the SOA, S_{act} is the area of the active section of the SOA. Moreover, we also suppose in this case that the carrier density \bar{N} is constant along the SOA. These hypothesis are equivalent to consider that the amplified spontaneous emission does not saturate the gain. A verification of this assumption will be shown in section 3. Under these conditions, a measurement of the small signal modal gain Γg_0 versus I will be equivalent, owing to Eq. 5, to a determination of the modal gain Γg versus \bar{N}/τ_s . Here, Γ is the ratio S_{act}/S_{guide} of the active to modal gain areas in the SOA.

A last relationship between $\frac{\bar{N}}{\tau_s}$ and U is then required to determine the modal gain Γg as a function of U . It is obtained by substituting $\Gamma g(\frac{\bar{N}}{\tau_s})$ in the saturated steady state solution of the carriers rate equation (Eq. 1):

$$\frac{I}{q L S_{act}} - \frac{\bar{N}}{\tau_s} - \frac{\Gamma g(\frac{\bar{N}}{\tau_s}) U}{\hbar \omega \Gamma} = 0, \quad (6)$$

where the injected current I is now fixed by the operating conditions.

Added to the previous relationship between Γg and $\frac{\bar{N}}{\tau_s}$, the Eq. 6 gives another expression of Γg as a function of $\frac{\bar{N}}{\tau_s}$, $\frac{U}{\Gamma}$ and I . Consequently, Γg and $\frac{\bar{N}}{\tau_s}$ can be known with respect to the local intensity $\frac{U(z)}{\Gamma}$ and the injected current I .

To solve Eq. 4, we need to express \bar{N} as a function of $\frac{U(z)}{\Gamma}$ and I . This is equivalent to express \bar{N} with respect to $\frac{\bar{N}}{\tau_s}$ since $\frac{\bar{N}}{\tau_s}$ is known as a function of $\frac{U(z)}{\Gamma}$ and I . Consequently, we model our SOA using the well-known equation [23]:

$$\frac{\bar{N}}{\tau_s} = A\bar{N} + B\bar{N}^2 + C\bar{N}^3, \quad (7)$$

where A , B , and C , which are respectively the non-radiative, spontaneous and Auger recombination coefficients, are the only parameters that will have to be fitted from the experimental results.

Using Eq. 7 and the fact that we have proved that \bar{N}/τ_s and Γg can be considered as function of $\frac{U(z)}{\Gamma}$ and I only, we see that \bar{N} , $\Gamma a = \Gamma \frac{\partial g}{\partial \bar{N}}$, and $\frac{U_s}{\Gamma} = \frac{\hbar \omega}{\Gamma a \tau_s}$ can also be considered as functions of $\frac{U(z)}{\Gamma}$ and I . This permits to replace Eqs. (3) and (4) by the following system:

$$\frac{dU}{dz} = U \left[-\gamma + \Gamma g\left(\frac{U(z)}{\Gamma}, I\right) \right], \quad (8)$$

$$\frac{dM}{dz} = M \left\{ -\gamma + \Gamma g\left(\frac{U(z)}{\Gamma}, I\right) \left[1 - \frac{\Gamma U / U_s\left(\frac{U(z)}{\Gamma}, I\right)}{1 + \Gamma U / U_s\left(\frac{U(z)}{\Gamma}, I\right) - i\Omega \tau_s\left(\frac{U(z)}{\Gamma}, I\right)} \right] \right\}. \quad (9)$$

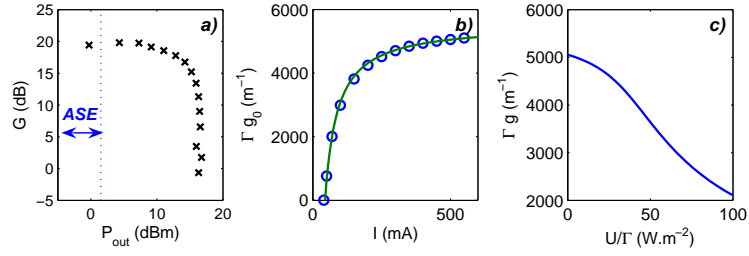


Fig. 1. (a) Experimental fiber-to-fiber gain G with respect to the output optical power P_{out} at a strong current (500 mA). The double arrow indicates the range of the measured ASE output power. (b) Experimental small signal gain Γg_0 as a function of the injected current I at 1535 nm, and fitted by: $\Gamma g_0 = C_1 - \frac{C_2}{I}$, with $C_1 = 5588.7 m^{-1}$ and $C_2 = 306.1 A^{-1} \cdot m^{-1}$. (c) Deduced material modal gain $\Gamma g(U)$ as a function of the local intensity U at 500 mA.

Eqs. (8) and (9) are then numerically solved: Eq. 8 gives $\frac{U(z)}{\Gamma}$, with the initial condition $\frac{U(0)}{\Gamma} = \sqrt{\gamma_i \frac{P_{in}}{S_{act}}}$, where P_{in} is the optical input power. $\frac{U(z)}{\Gamma}$ can be then introduced into Eq. 9, and the microwave transfer function of the SOA $S_{21} = \gamma_i \frac{M(L)}{M(0)}$, where γ_i are the insertion losses, is then computed. If the output power of the RF microwave signal is wanted, $P_{RF} = 2R\eta_{ph}^2 \gamma_i \left| \frac{mP_{in}M(L)}{2} \right|^2$, with the initial condition $M(0) = 1$, where m the input modulation index, and R and η_{ph} are respectively the photodiode resistive load and efficiency.

The microwave complex transfer function S_{21} fully characterizes the slow light properties of the SOA. Indeed the optical group delay $\Delta\tau_g$ can be expressed as $\Delta\tau_g(\Omega) = \frac{arg(S_{21}(\Omega))}{\Omega}$, and the group index $\Delta n_g(\Omega) = \frac{c}{L} \frac{arg(S_{21}(\Omega))}{\Omega}$.

It is important to note that the recombination coefficients A , B and C are the only fitting parameters of our model. Once obtained from experimental data, they are fixed for any other experimental conditions. Moreover, the only geometrical required parameters are the length L of the SOA and the active area cross section S_{act} . The derivation of a predictive model, independent of the experimental conditions (current and input optical power) is then possible, provided that the simple measurements of the total losses and the small signal gain versus the current are conducted. The above model lies in the fact that first, the spatial variations of the saturation parameters are taken into account, and second, their values with respect to the local optical power are deduced from a simple measurement. These keys ideas lead to a very convenient model of the microwave complex transfer function of the SOA, and then of the slow light properties of the component. It can be easily used to characterize commercial components whose design details are usually unknown, as we will experimentally show in the next section.

3. Experiment

In order to validate our model, we studied a commercially available SOA (InP/InGaAsP Quantum Well Booster Amplifier from COVEGA). The length L of this SOA is 1.50 mm and the active area cross-section is set at $0.06 \mu m^2$. We proposed to compare the experimental and simulated complex transfer function S_{21} for a large set of operating conditions (P_{in}, I). As explained in section 2, the study of the phase $arg(S_{21})$ is equivalent to the optical group delay. We can then restrain our comparison to S_{21} . In order to fully characterize the response of the SOA through $\Gamma g(U)$ as described in section 2, the preliminary step consists in measuring the total losses and the unsaturated gain $\Gamma g_0(I)$ for different injected currents.

The total losses are measured by the following experiment: at low current, the output optical power is measured while a strong input optical power is sent into the SOA. When the current

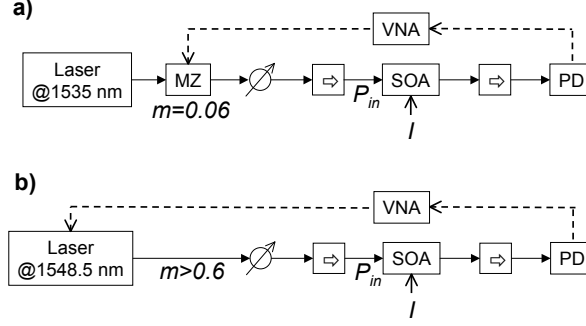


Fig. 2. Experimental set-up. For small modulation index m , a laser is externally modulated by a Mach-Zehnder modulator (MZ) (a); for large modulation index, a directly modulated laser is used (b). In both cases, the input optical power P_{in} is controlled through a variable optical attenuator; two optical isolators are used before and after the SOA. The photodetector (PD) restitute the RF signal. The Vector Network Analyser (VNA) is calibrated with the whole link without the SOA, in order to measure the RF transfer function of the SOA.

is low enough, the SOA is in the absorption regime: the resulting output power is an increasing function of the input power (absorption saturation). When the current is above the transparency current, the resulting output power becomes a decreasing function of the input power (gain saturation). Between these two regimes, i.e. at transparency, the ratio between the output power and the input power is exactly equal to the total losses. The total losses of the SOA $\gamma_i \exp(-\gamma L)$ are measured to be equal to -16.4dB in our case.

To measure only the unsaturated gain Γg_0 despite the amplified spontaneous emission, we measured the SOA unsaturated RF gain G_{RF} ($=|S_{21}|^2$) at a RF frequency Ω well above $1/\tau_s$ (typically 20 GHz). The derivation of the modal gain Γg with respect to $\frac{N}{\tau_s}$ from the unsaturated gain $\Gamma g_0(I)$ is relying on the hypothesis that the amplified stimulated emission (ASE) does not saturate the gain. In Fig. 1a, we represent the experimental fiber-to-fiber gain with respect to the output optical power at a strong current (500 mA) and the range of the experimental output power of the ASE. The maximum power of the ASE is equal to 1.54 dBm. Moreover, when the small signal measurement is performed, a maximum input optical power of $80 \mu\text{W}$ was used, corresponding to an output optical power of 8.1 dBm for the maximum current. Consequently, both signal and ASE output power level are well below the output power required to saturate the gain (14.2 dBm for a 3dB gain reduction). Therefore, the experimental conditions match our preliminary assumptions. Under these conditions, Eq. 8 can be simplified and integrated, leading to the expression of the optical small signal gain Γg_0 : $\exp(\Gamma g_0 L) = \frac{\sqrt{G_{RF}}}{\gamma_i \exp(-\gamma L)}$. As shown in Fig. 2a, we used a Vector Network Analyzer (VNA) to measure the RF gain G_{RF} for a small input power which does not saturate the SOA (typically $10 - 80 \mu\text{W}$). The unsaturated gain of our SOA is displayed in Fig. 1b. It is empirically fitted by $\Gamma g_0 = C_1 - \frac{C_2}{I}$ with a good agreement. From this simple measurement and using Eq. 6, the material modal gain Γg is then known as a function of the local intensity U/Γ inside the SOA (Fig. 1c).

The complex RF transfer function of the SOA is measured thanks to a VNA for small and large modulation indices (set-ups in Fig. 2). In Fig. 3 and Fig. 4, we report the corresponding RF gains, $20 \log |S_{21}|$, and the measured evolution of the RF phase shift, $\arg(S_{21})$, as a function of the modulation frequency Ω . In each of these figures, the plots labeled (a) and (b) correspond to the evolutions of the RF gains and phase shifts versus RF frequency, for different injected currents, while the plots labeled (c) and (d) are obtained by managing the input optical power.

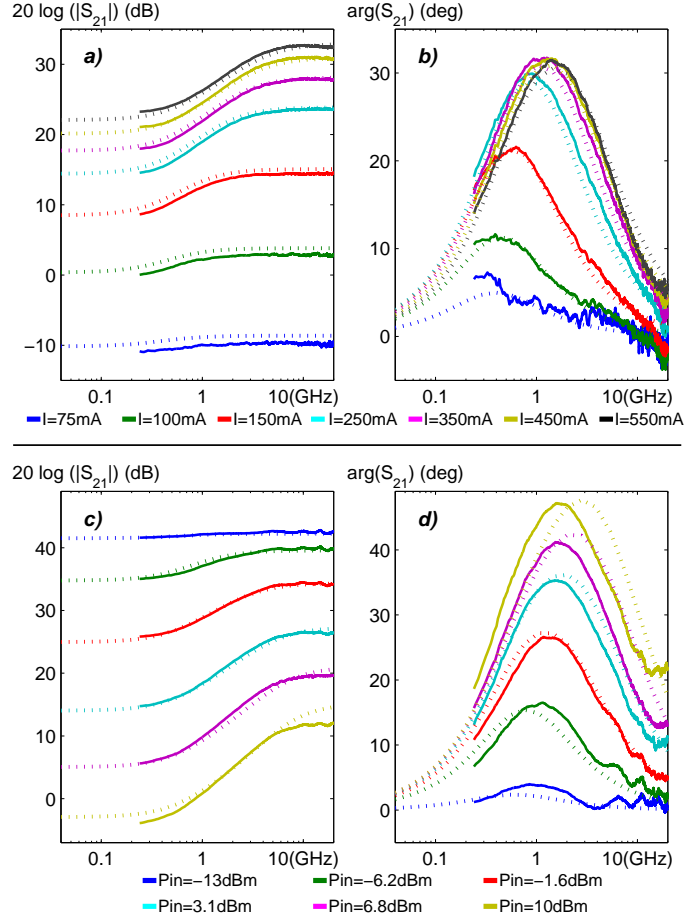


Fig. 3. Low modulation index ($m = 0.06$) : gain and phase shift simulations (dashed line) and experimental data (solid line) for (a) and (b): different injected currents at $P_{in} = 0\text{dBm}$, and for (c) and (d): different optical input powers P_{in} at $I = 500\text{mA}$. The operating wavelength was 1535nm .

4. Discussion

In Fig. 3 and Fig. 4, the simulation results are reported in dashed line. The best fit values for the recombination coefficients are: $A = 2 \times 10^9\text{s}^{-1}$, $B = 1.2 \times 10^{-10}\text{cm}^3\text{s}^{-1}$, $C = 1.8 \times 10^{-31}\text{cm}^6\text{s}^{-1}$. These values are in the range of what can be found in the literature for semiconductor materials [25, 26, 27, 28]. The computed complex transfer function shows a very good agreement with the experimental data, both at small and large modulation index, for any experimental conditions (injected current, input optical power), and with a single set of the fitting parameters (A, B, C): our convenient model is predictive for any experimental conditions.

In order to highlight the weight of the spatial variations of the carrier density and the saturation parameters, we plotted in Fig. 5a,5b the variations of the carrier density \bar{N} along the SOA for the different experimental situations of Fig. 3. The subsequent variations of the modal gain Γg and the saturation parameters P_s , τ_s and a , with respect to \bar{N} , are displayed in Fig. 5c,5d. We find at least one order of magnitude of variation for almost all these parameters, which are

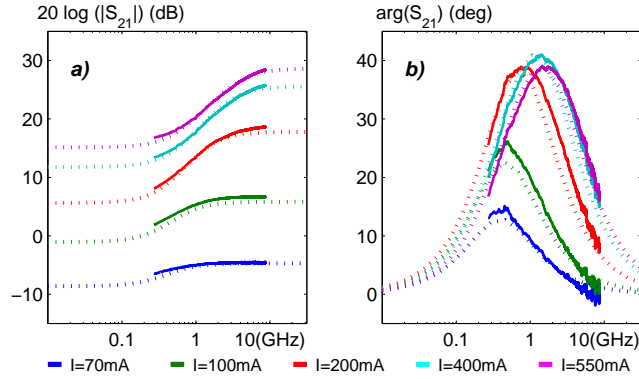


Fig. 4. Large modulation index ($m > 0.6$) : gain and phase shift simulations (dashed line) and experimental data (solid line) for (a) and (b): different injected currents at $P_{in} = 0$ dBm. The operating wavelength was 1548.5nm.

nevertheless often taken constant in literature for practical models [5, 14, 20, 21]. According to Eq. 7, this approximation can be justified when the variations of \bar{N} along the SOA are relatively not too strong, that is for moderate bias current (< 150 mA in our case) or a high bias current, but low optical power. However, for any other condition, and especially in the case of quantum well or quantum dots structures, it is necessary to take into account the saturation dynamics along the propagation to ensure good performances of the model and robustness versus changes in experimental conditions. Indeed, Fig. 5 shows that considering P_s , τ_s and a constant, and then Γg linear with \bar{N} , drastically limits the range of experimental conditions (P_{in}, I) where such models are valid, which forces the saturation parameters to be adjusted with the current and/or the optical input power.

Our improved model is still easy to use, even for commercial components, but despite the hypothesis we were compelled to make, it remains valid for a large range of experimental conditions, with a reduced set of unknown - and thus fitted- parameters. These advantages have been achieved by taking into account the spatial variation of the saturation parameters and by showing that their values as a function of the local optical power can be retrieved from a simple measurement. It ensures that the model only relies on material fitting parameters, independent of the optical intensity and injected current.

The slow light properties are then also modeled for a large range of the input optical powers P_{in} and injected currents I , which is essential from the operational point of view, since the speed of light in SOA is controlled by these two key parameters. While the applications of slow light in SOA are taking shape, a convenient and accurate model with the parameters tuning the delays is a necessary tool to fully characterize the effect of slow light in SOA on a microwave link, or to develop new architectures improving the slow light properties. This model could be easily used when an optical filtering is performed after the SOA to enhance the slow light effect, as described in [20, 29]. In this case, Eq. 9 just has to be replaced by the corresponding coupled equations in E_1 and E_2 . Moreover, to take into account higher order coherent population oscillations [30], the present model can be generalized using equations similar to Eq. 9 for each harmonic of the optical intensity. The determination of Γg as a function of U is slightly more subtle in this case: it is presented in another paper, in order to study the harmonic generation and the intermodulation products [31].

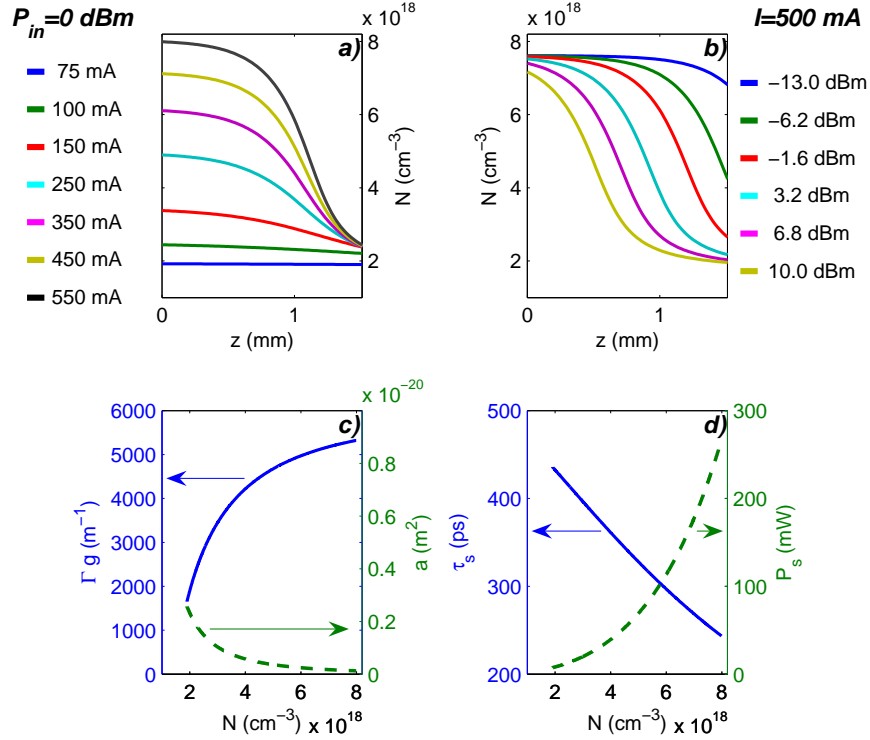


Fig. 5. (a) and (b): Simulated carrier density \bar{N} along the SOA: (a) at a fixed input optical power (0 dBm), for various currents; (b) at a fixed current (500 mA), for various input optical power. (c) and (d): Simulated variations with respect to the carrier density \bar{N} of (c) the modal gain Γ_g (solid line), and the modal differential gain a (dashed line); (d) the carrier lifetime τ_s (solid line), and the local saturation power P_s (dashed line).

5. Conclusion

We developed an improved but still convenient model in order to predict the RF behavior and slow light properties of the SOA, valid for any experimental conditions (input optical power, injected current). It takes into account the spatial variations of the saturation parameters along the SOA, which are fully characterized by the simple measurement of the small signal gain. The resulting model only relies on material fitting parameters, independent of the optical intensity and injected current. We showed a remarkably good agreement between the model and the experimental data, at small and large modulation indices. The ease of use and the accurate prediction obtained for any experimental conditions will be useful to characterize the effect of slow light in SOA on a microwave link, and to develop new designs improving the slow light properties. The key ideas of this improved model can easily be used when optical filtering is performed after the SOA. A generalization of our approach will be carried out in a next step, in order to determine the harmonic generation, intermodulation products and spurious free dynamic range, for a full characterization of a SOA based opto-electronic link.

Acknowledgments

The authors acknowledge the partial support from the "Délégation Générale pour l'Armement" DGA/MRIS and from the GOSPEL EC/FET project.